Mapping the Mottness under Magnetic Field

Lei Wang (lw2379@columbia.edu)
Nanjing University https://orcid.org/0000-0002-1919-9107

LingNan Wei
Nanjing University

Zhao-Long Gu
Nanjing University

Ammon Fischer
RWTH Aachen University

YangChen He
University of Wisconsin

Qiaoling Xu
Songshan Lake Materials Laboratory

Augusto Ghiotto
Columbia University https://orcid.org/0000-0003-0860-9817

Clara Weber
RWTH Aachen University https://orcid.org/0000-0002-6779-7136

Kenji Watanabe
National Institute for Materials Science https://orcid.org/0000-0003-3701-8119

Takashi Taniguchi
National Institute for Materials Science, Tsukuba, Ibaraki https://orcid.org/0000-0002-1467-3105

Martin Claassen
University of Pennsylvania

Angel Rubio
Max Planck Institute for the Structure and Dynamics of Matter https://orcid.org/0000-0003-2060-3151

Andrew Millis
Columbia University

Abhay Pasupathy
Columbia University https://orcid.org/0000-0002-2744-0634

Lede Xian
Max Planck Institute for the Structure and Dynamics of Matter https://orcid.org/0000-0002-9595-2404

Daniel Rhodes
University of Wisconsin - Madison https://orcid.org/0000-0002-7651-3211

Dante Kennes
RWTH Aachen University

Jian-Xin Li
Nanjing University https://orcid.org/0009-0007-3901-8119

Physical Sciences - Article

Keywords:

Posted Date: October 9th, 2023

DOI: https://doi.org/10.21203/rs.3.rs-3385782/v1

Additional Declarations: There is **NO** Competing Interest.

Mapping the Mottness under Magnetic Field

LingNan Wei[1†], Zhao-Long Gu[1†], Ammon Fischer[2], YangChen He[3], Qiaoling Xu[4], Augusto Ghiotto[5], Clara S. Weber[2], Kenji Watanabe[6], Takashi Taniguchi[7], Martin Claassen[8], Angel Rubio[9,10], Andrew J. Millis[5,10], Abhay N. Pasupathy[5,11], Lede Xian[4,9], Daniel A. Rhodes[3*], Dante M. Kennes[2,9*], Jian-Xin Li[1,12*], and Lei Wang[1,12*]

[1] *National Laboratory of Solid-State Microstructures, School of Physics, Nanjing University, Nanjing 210093, China*

[2] *Institut für Theorie der Statistischen Physik, RWTH Aachen University and JARA-Fundamentals of Future Information Technology, Aachen 52056, Germany*

[3] *Department of Materials Science and Engineering, University of Wisconsin, Madison, WI, USA*

[4] *Songshan Lake Materials Laboratory, Dongguan, Guangdong 523808, China*

[5] *Department of Physics, Columbia University, New York, NY 10027, USA*

[6] *Research Center for Electronic and Optical Materials, National Institute for Materials Science, 1-1 Namiki, Tsukuba 305-0044, Japan*

[7] *Research Center for Materials Nanoarchitectonics, National Institute for Materials Science, 1-1 Namiki, Tsukuba 305-0044, Japan*

[8] *Department of Physics and Astronomy, University of Pennsylvania, Philadelphia, PA 19104, USA*

[9] *Max Planck Institute for the Structure and Dynamics of Matter, Center for Free-Electron Laser Science (CFEL), Luruper Chaussee 149, Hamburg 22761, Germany*

[10] *Center for Computational Quantum Physics, Simons Foundation Flatiron Institute, New York, NY 10010 USA*

[11] *Condensed Matter Physics and Materials Science Division, Brookhaven National Laboratory, Upton, New York 11973, USA*

[12] *Collaborative Innovation Center of Advanced Microstructures, Nanjing University, Nanjing 210093, China*

[†] *These authors contributed equally. and*

[*] *Corresponding authors, Email: darhodes@wisc.edu; dante.kennes@mpsd.mpg.de; jxli@nju.edu.cn; leiwang@nju.edu.cn*

Charge and spin are two intrinsic degrees of freedom of an electron. In a Mott insulator (MI), they are separated in that the charge degree is frozen due to strong Coulomb interaction U while the spin degree can still fluctuate and is governed by the energy scale of spin exchange $J \simeq 4t^2/U$ (t, hopping integral). Usually, a magnetic field can only manipulate the spin degree as the attainable Zeeman energy E_z can only compete with J at the scale of tens of milli-electron volts, while it does not affect the charge degree with U being at least two orders of magnitude larger [1–3]. Therefore, the complete evolution of a Mott insulator under magnetic field with both charge and spin impacted has yet to be explored. With recent progress in two-dimensional (2D) moiré systems, Mott insulators have been realized with significantly reduced U [4–9], providing an opportunity to investigate this problem. Here, we map out the full picture of Mottness under magnetic field by transport measurements on twisted bilayer (TB) WSe_2 with twist angle θ ranging from 2.4° to 3.2°. We achieve the tuning of the charge dynamics of the Mott insulator using magnetic fields and observe unexpected Mott insulator-metal-Mott insulator (IMI) transitions. We theoretically establish that these IMI transitions are driven by an exotic form of spectral weight transfer (SWT) between the spin-split Hubbard bands due to carrier occupancy variations of different spins. We further identify the reentrant insulating phase at higher magnetic fields as a Mott-Zeeman insulator (MZI) with its gap determined collectively by U and E_z. Remarkably, with SWT, the observed critical magnetic field for this reentrance is as low as 5 T, which corresponds to a Zeeman energy approximately an order of magnitude smaller than U. The unveiled IMI transitions experimentally and theoretically evidence SWT as a crucial driving mechanism for the evolution of a Mott insulator in response to control parameters, which offers an unprecedented perspective into the nature of Mott physics.

The spin degree of freedom usually leads to a two-fold degeneracy of an electronic band, with each energy level harboring spin up and spin down quantum states. A magnetic field breaks this degeneracy, resulting in a band splitting with $E_Z \sim g\mu_B B$ (g, g-factor; μ_B, Bohr magneton; B, magnetic field). For a single-particle band, there is only one characteristic energy scale given by the bandwidth w, as the charge and spin degrees of freedom are not separated. If E_Z is greater than w, the system would be fully spin polarized and turns into a band insulator with a charge gap at half-filling. On the other hand, for a correlated band in a Mott insulator, the charge and spin degrees of freedom are associated with two separate energy scales, U and J. In previous studies, magnetic fields have been used to successfully manipulate the spin structures [10–13], but with the charge degree left unaffected due to a larger energy scale of U ($\sim$ eV). In order

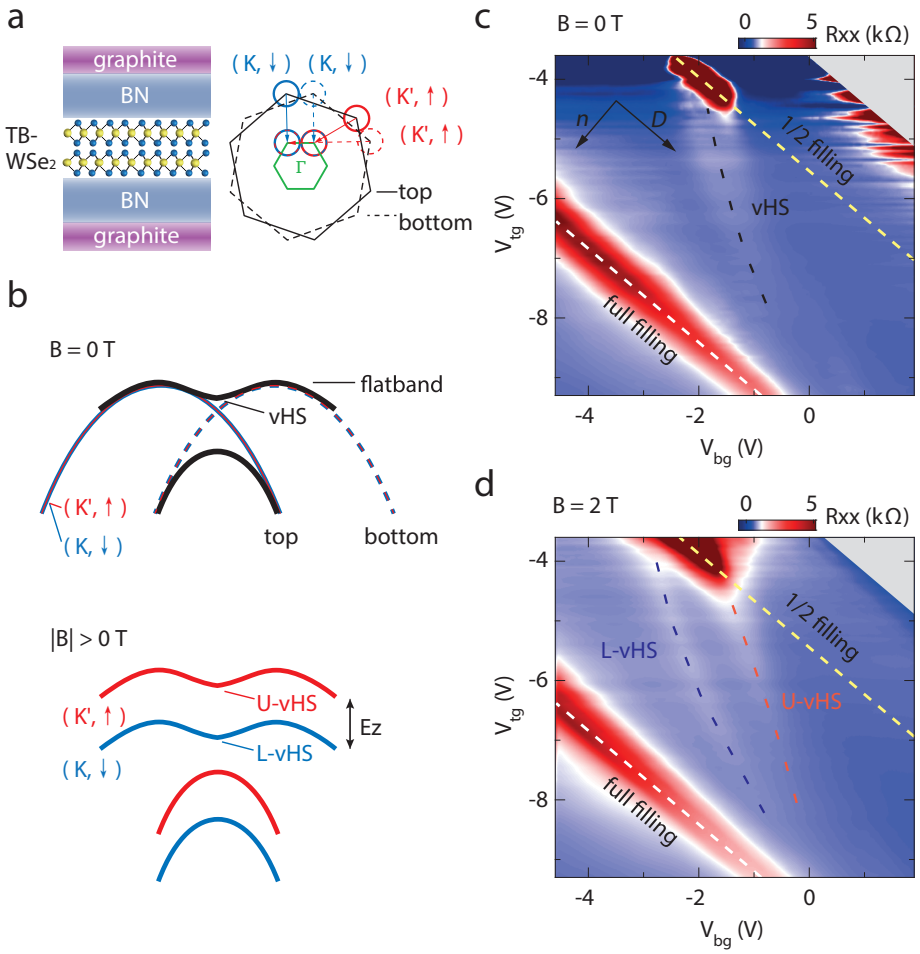

FIG. 1. **Tunable flat bands, correlated insulating states and vHS in TB-WSe_2. a,** Left: Schematic of a dual-gated TB-WSe_2 device. Right: Brillouin zones of the top (solid line) and bottom (dashed line) layers. The states near K and K′ are shown as blue and red, respectively. The resulting moiré Brillouin zone is shown as green. **b,** Schematics of the TB-WSe_2 valence band structure under zero magnetic field (top) and finite (down) out-of-plane magnetic field. The red (blue) curve represents the spin-up (down) band locked to K′ (K) valley. With magnetic field, the single-particle valence band splits into two bands separated by Zeeman energy E_Z, and the single vHS turns into an uppper-vHS (U-vHS) and lower-vHS (L-vHS). **c-d,** Longitudinal resistance, R_{xx}, as a function of back-gate (V_{bg}) and top-gate (V_{tg}) voltages at 0 T and 2 T, respectively (T = 1.5 K).

for E_Z to match this charge gap scale, an infeasibly large magnetic field in excess of 10,000 T would be required.

Physically, the Mott insulator differs from a band insulator in that the states in the lower Hubbard band (LHB) and upper Hubbard band (UHB) relies on carrier occupancy [1, 2], while a single-particle band is trivially irrelevant to its occupancy. In this way, when the magnetic field breaks the spin degeneracy, the occupancy of the spin-split sub-LHBs and sub-UHBs are simultaneously changed. Consequently, the reconstruction of Hubbard bands will occur, and exotic correlated physics sparkled by magnetic field may emerge.

Recently, two-dimensional (2D) moiré heterostructures have emerged as potential candidates to investigate this regime [14]. Mott insulators have been reported at half filling of a moiré flat band in twisted transition metal dichalcogenides (TMDs) [7–9, 15–17]. In particular, AA-stacked TB-WSe_2 devices between 4° and 5° twist have been shown to have moderate correlation, with U and w around 100 meV [7]. In principle, U and w in TB-WSe_2 can be continuously varied and further reduced by pushing to smaller twist angles [7]. Here we present a series of dual-gated TB-WSe_2 devices (see Method for fabrication details) around 3° twist angle (Fig.1a), where we are able to further reduce the bandwidth w down to ∼30 meV (Fig.1b and Extended Data Fig.1), with a similar U [7]. In combination with a large g-factor in WSe_2 [18, 19], for the first time we can successfully tune the charge dynamics in a Mott insulator with magnetic field. We find that the Mott insulator transitions into a MZI with po-

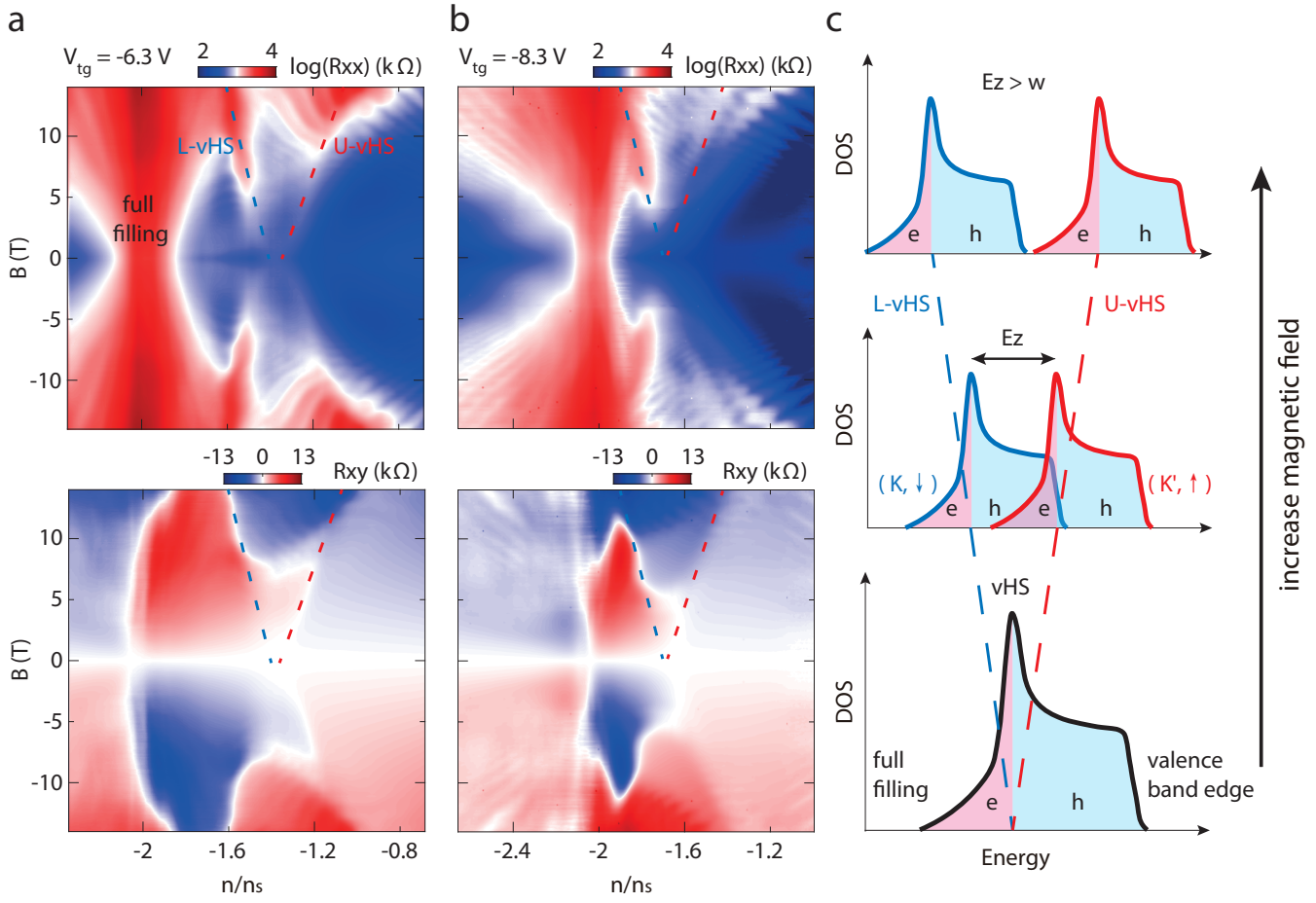

FIG. 2. **Zeeman effect on the single-particle band structure with vHS near full filling in TB-WSe_2. a-b,** Longitudinal resistance (top) and Hall resistance (bottom) versus normalized carrier density n/n_s and magnetic field, B, with V_{tg} fixed at -6.3 V and -8.3V, respectively. The dashed blue (red) lines mark L-vHS (U-vHS). **c,** Evolution of the density of states (DOS) of the top moiré valence band versus energy as B increases. The blue (red) dashed lines track the positions of the L-vHS (U-vHS). When $B = 0$ T, spin-up and spin-down bands are degenerate, exhibiting only one vHS. When $B \neq 0$ T, the Zeeman effect breaks this degeneracy, thus two vHSs appear. When B is large enough ($E_Z > w$), the two subbands will eventually move apart completely. For illustration, the Landau splitting is not considered.

larized spins at a surprisingly low magnetic field, whose E_Z is only a fraction of U. Between the two insulators, we find that the charge gap can be reduced to zero within an extended range of displacement fields, resulting in an unexpected intermediate metallic phase. Based on cluster perturbation theory (CPT) [20–22] complemented by the mean-field calculations of the moiré Hubbard model [23–27], we find these exotic phenomena are attributed to a novel type of SWT. Such spectral weight transfer in a magnetic-field-induced phase transition is a generic feature of the Mottness.

Tunable vHS from half filing to full filling

The resistance of a $\theta \sim 3.2°$ sample measured at $T = 1.5$ K is shown as a function of top (V_{tg}) and bottom (V_{bg}) gate voltages in Fig. 1c. As compared to larger values of θ examined in previous works [7], the full-filling ($n/n_s = -2$) band insulator and the half-filling ($n/n_s = -1$) Mott insulator shift to lower carrier densities and can both be observed within the achievable gate voltage ranges allowed by the hBN encapsulation. We also observe a series of resistance peaks (marked by the black dashed line), which are attributed to van Hove singularities (vHSs) that move from half filling towards full filling as the displacement field (D) increases [23]. These unique features enable investigations into how a single-particle band and a correlated band behave under a magnetic field at the same time.

Single particle band splitting

At $B = 2$ T, we find that the single vHS trace from Fig. 1c splits into two, a lower and a upper vHS (Fig. 1d). This splitting represents the Zeeman splitting of the single-particle spin-degenerated moiré subband (Fig. 1b).

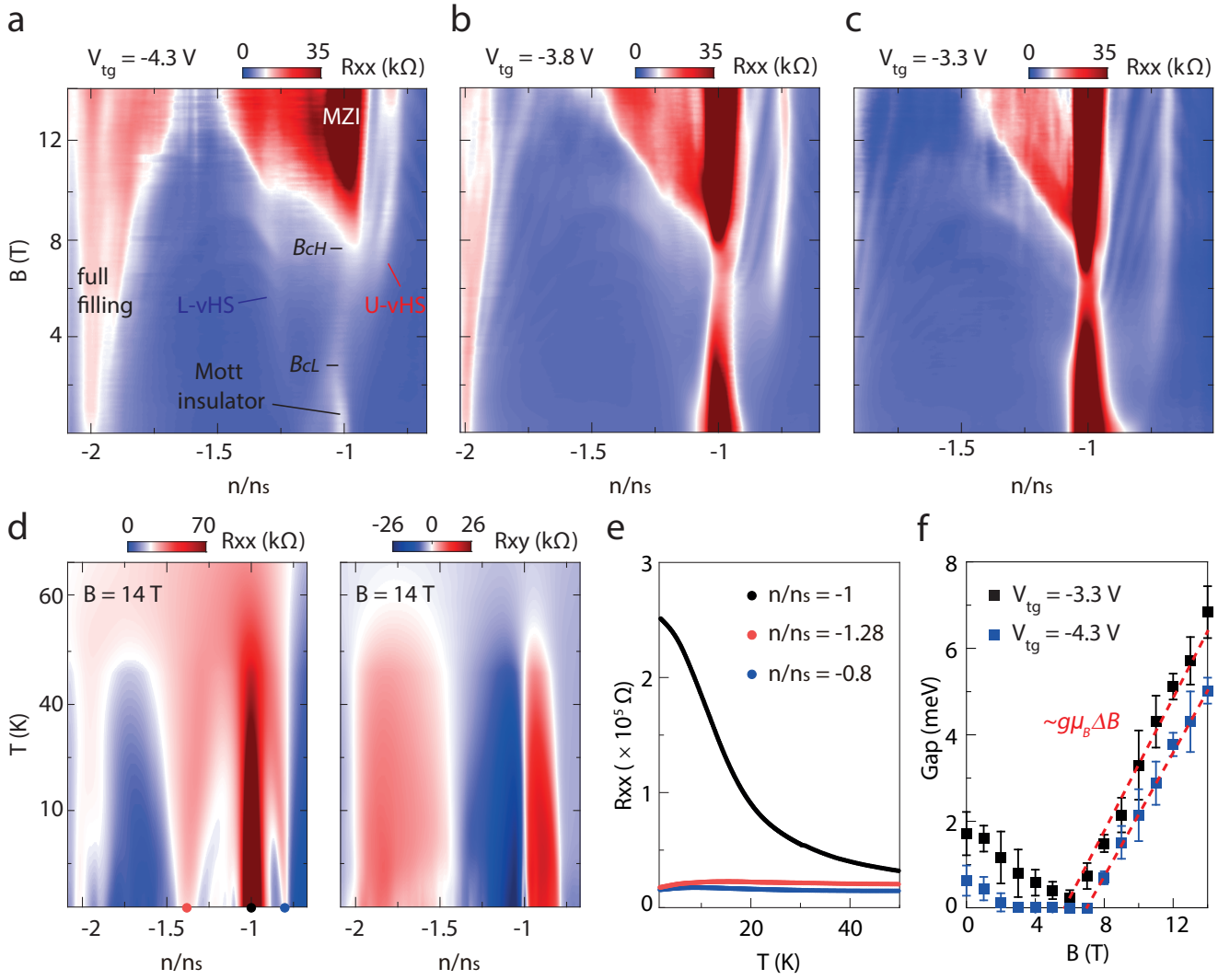

FIG. 3. **Magnetic field response of the Mott insulator. a-c,** R_{xx} versus n/n_s and B with V_{tg} fixed at -4.3 V, -3.8 V, and -3.3 V, respectively. With magnetic field, the resistance of the Mott insulator drops for B between 0 T and B_{cL}, and another insulating state at half filling re-enters for $B > B_{cH}$. **d,** R_{xx} and R_{xy} maps as functions of T and n/n_s with $V_{tg} = -4.3$ V, $B = 14$ T. The red, black, and blue points mark the positions of L-vHS, half filling, and U-vHS, respectively. **e,** R_{xx} versus T at the red, black and blue points marked in **d**. The state at half filling shows an insulating behavior. **f,** Insulating gap at half filling versus B with V_{tg} at -3.3 V and -4.3 V. Error bars represent the uncertainty that arises from determining the linear (thermally activated) regime for the fit. The red dashed lines indicate a Zeeman-like linearly increasing energy with $g \simeq 15$.

Converting the splitting in carrier density to energy, we can estimate a g-factor of ∼11 in the applied D range (Extended Data Fig.2), which is similar to the previously reported values for few-layer WSe_2 [18, 19].

Fig. 2a-b show the fan-diagrams for the longitudinal resistance R_{xx} (top panels) and Hall resistance R_{xy} (bottom panels) of a 3.2° sample for fields between -14 T and 14 T, at two different V_{tg} values (-6.3 V and -8.3 V), where the vHSs are all near the full filling. Owing to the Zeeman effect, we observe a linear increase, with respect to B, in the separation between L- and U-vHSs. At $B \sim 0$ T, R_{xy} exhibits a single sign change at the vHS, consistent with the expected response for a single band where the dispersion changes from hole-like to electron-like as the band is filled (Fig. 2c bottom). For larger B, as the vHS bifurcates R_{xy} shows either a sign change or an abrupt change of magnitude across the L-vHS and U-vHS traces (see similar data on other devices in Extended Data Fig.3). This behavior is due to a mixture of electron-like (from the spin-up subband) and hole-like (from the spin-down subband) carriers between the L-vHS and U-vHS (Fig. 2c middle). In this region, whether

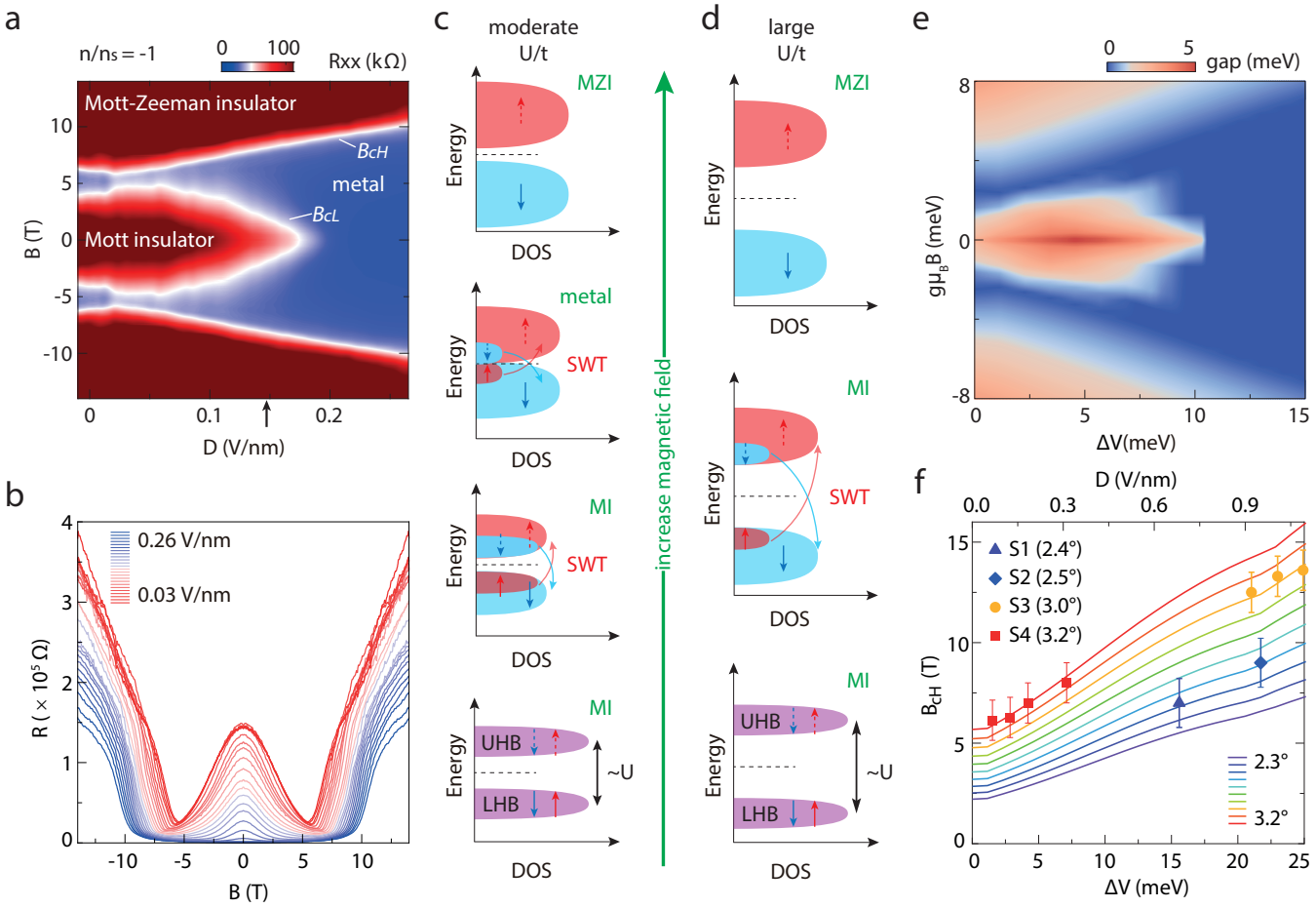

FIG. 4. **Spectral-weight-transfer driven transitions to the Mott-Zeeman insulator at half filling. a,** R_{xx} map as a function of displacement field, D, and B at half filling ($T = 1.5$ K). Black arrow indicates the crossover from large to moderate U/t regimes as D increases. **b,** Line-cuts of **a** at typical D values. **c,** Schematic for the evolution of the spin-resolved DOS of LHB and UHB with B in the moderate (left) and large (right) U/t regimes. Purple shading represents the spin-degenerate LHB and UHB, which are separated by the Hubbard interaction U, at $B = 0$ T. Red (blue) shading represents the split spin-up (down) sub-Hubbard bands at $B > 0$ T. The shape of the DOS drawn here is illustrative (see Extended Data Fig.8 and Fig.9 for the numerical results). **d,** Theoretical phase diagram mapped by the energy gap versus layer potential difference $\Delta V(\propto D)$ and E_Z calculated by CPT. **e,** Higher critical field B_{cH} versus ΔV (bottom axis) and D (top axis) at different twist angles. Lines represent the CPT results and points represent the experimental data.

the response in R_{xy} is overall electron-like or hole-like depends on the details of how the two spin-polarized subbands overlap. Fig. 2c (top) depicts the fully polarized criteria for this single-particle band, which requires E_Z to be greater than w (30 meV), corresponding to $B \sim 50$ T (using a g-factor of 11).

Observation of the Mott-Zeeman insulator

Next we move to the magnetic field response of the correlated Mott-Hubbard band. Figures 3a-c show R_{xx} (corresponding R_{xy} in Extended Data Fig.4) versus n/n_s and B at three different V_{tg} values (-3.3 V, -3.8 V, and -4.3 V), where the vHSs are all around half filling. As B increases from 0 T to a critical value (B_{cL}), the resistance of the Mott insulator decreases. Increasing B further, we observe another critical field (B_{cH}), beyond which a new state emerges at half filling whose resistance abruptly increases with B. To check the insulating nature of this new state, we measure the temperature dependence of R_{xx} and R_{xy} at 14 T (Fig. 3d). At low temperatures, the R_{xy} changes sign four times: two times at half filling and full filling, suggesting a reset of the carrier density at the charge gaps; and the other two times at the L-vHS and U-vHS points, owing to changes in the band curvature across the singularity point. The R_{xx} at half filling (marked by the black dot) shows a thermally activated behavior (black dot in Fig. 3e), confirming the charge gap. The L-vHS and U-vHS on the two sides of half filling peak, despite having resistance peaks over 10 kΩ, both exhibit metallic behavior with resistance increasing as T increases (red and blue dots in Fig. 3e).

To investigate the evolution of the Mott insulator, we further extract the gap size as a function of magnetic field (Fig. 3f) by measuring a series of R_{xx} versus T at every 1 T (see Extended Data Fig.5 for fittings of the activation curves). When V_{tg} equals to -4.3 V, the blue squares show that the sample undergoes IMI phase transitions. When B approaches B_{cL} from 0 T, the insulating gap gradually decreases to zero. When $B > B_{cH}$, the charge gap linearly increases with B (extracted g factor ~ 15), indicating the spin polarized nature. Remarkably, B_{cH} is surprisingly small (~ 7 T). Moreover, we find that the higher-B insulator cannot be explained from a single-particle band structure calculation alone (Extended Data Fig.6), highlighting the relevance of correlations. Together with further theoretical evidences to be presented in the next section, we dub it a *Mott-Zeeman insulator*.

When V_{tg} equals to -3.3 V (black squares in Fig. 3f), the bandwidth of the moiré flat band is narrower than that in $V_{tg} = -4.3$ V as D decreases [7], resulting in a larger U/t. In this case, though the insulating gap shows a similar decreasing-increasing trend with B, the minimum gap is finite while it is close to zero, exhibiting an insulator-to-insulator (II) transition without an intermediate metallic phase.

The complete IMI/II transitions as a function of B and D are summarized in Fig. 4a (corresponding R_{xy} in Extended Data Fig.7) and the detailed resistance line-cuts are presented in Fig. 4b. The region of the Mott insulator enclosed by B_{cL} shrinks as both B and D increase. In contrast, B_{cH} increases with D, exhibiting an interesting linear dependence. As a result, the metallic state in the IMI transitions spans a wider range of B for larger D fields. Noticeably, even for $D \gtrsim 0.2$ V/nm, at which point the Mott insulator transitions into a metallic state without magnetic field, the MZI continues to exist.

Spectral weight transfer in spin-split Hubbard bands

To further understand the mechanism of the observed IMI/II transitions and the nature of the MZI, we employ CPT (Extended Data Fig.8) and mean field (Extended Data Fig.9) analyses to reveal the evolution of the spin-resolved DOS for correlated electrons with magnetic field in the Mott insulating phase. The results are summarized by the cartoon shown in Fig. 4c and d, corresponding to the moderate and large U/t cases, respectively. Both the LHB and UHB split after B increases from zero. However, in stark contrast to the case of single-particle bands, the "area" (*i.e.*, the summed DOS) of every spin-split Hubbard band changes at the same time as B increases. Due to the sum rule that the total DOS of each spin from both LHB and UHB is conserved, this process is in fact a manifestation of the so-called "spectral weight transfer", *i.e.*, the spectral weight of up spins transfers from LHB to UHB as B grows. The response of down spins is exactly the opposite.

Spectral weight transfer is a unique feature of Mott insulators. Previously, such phenomenon has only been unveiled in the field of doped Mott insulators, where the spectral weights of both LHB and UHB transfer to the in-gap states when doping away from half-filling [1, 2, 22, 28, 29]. Here, we reveal a new type of SWT realized in Mott insulators under a magnetic field with the system fixed at half-filling, where the total spectral weight of both spins in each Hubbard band remains unchanged while the SWT occurs between the spin-split sub-LHBs and sub-UHBs, as shown in Fig. 4c and d.

SWT constitutes a fundamental difference between single-particle bands and Hubbard bands. Single-particle bands are the simple direct composition of single-particle states, while Hubbard bands reflect the occupancies of electrons at every lattice site due to the strong Coulomb repulsion between electrons. Actually, LHB is composed of singly-occupied states, while UHB is composed of doubly-occupied states. LHB and UHB are separated by the Hubbard interaction U. We notice that recent studies on Mott insulators under magnetic field have not made a difference between the Hubbard bands and single-particle bands, specifically, the field response of Hubbard bands were treated in the same way as the Zeeman splitting of single-particle bands [4]. In fact, Hubbard bands undergo comprehensive reconstructions via SWT in response to the magnetic field due to their intrinsic occupancy-dependent property.

When B is zero, the ground state of the system can be the 120° Neel state or a quantum spin liquid [30–33]. It contains equal probabilities of finding spin-up and spin-down electrons in the system (Fig. 4c and d bottom panels), resulting in a spin-degeneracy in LHB. Correspondingly, to create a doubly-occupied site above this ground state, equal probabilities of spin-up and spin-down electrons can be added to the system (dashed arrows in the bottom panels of Fig. 4c and d), leading to the spin-degeneracy in UHB.

When B is introduced, the Zeeman effect splits the degenerate spins in both LHB and UHB. Importantly, this leads to spin flips in the ground state from up to down. Such decrease in the spin-up electron number causes a decrease of the probability of finding a singly-occupied spin-up site in LHB (area shrinking). Due to the aforementioned sum rule, there is a simultaneous increase of the probability of adding a spin-up electron to create a doubly-occupied site in UHB (area expanding). This is right the SWT of spin-up bands from LHB to UHB (Fig. 4c middle two panels, Fig. 4d central panel). A similar analysis can be made for spin-down bands. This is completely different from the case of single-particle bands, where the spin-flip effect is only trivially manifested by the redistribution of carriers from a spin-up band to a spin-down band while the spectral weight of each spin-split single-particle band remains unchanged (Fig. 2c).

A natural consequence of the area expanding (shrink-

ing) of the sub-Hubbard bands driven by SWT is that their bandwidths become wider (narrower). Specifically, the bandwidths of the spin-down subband in LHB and the spin-up subband in UHB both increase, leading to a decrease of the charge gap. For the moderate U/t case, U is close to the bandwidth of the Hubbard bands at $B = 0$ T, thus, the charge gap can dwindle down to zero as a result of the bandwidth increase with B, leading to an intermediate metallic phase (Fig. 4c second topmost panel). On the other hand, for the large U/t case, U is much larger than the bandwidth of the Hubbard bands at all B-field values, the charge gap only decreases to a finite value exempting from the intermediate metallic state.

When B is sufficiently large (B_{cH}), the spectral weight is fully transferred (Fig. 4c and d top panels). Thus, the spin-up (-down) band disappears in LHB (UHB), resulting in a fully-spin-polarized insulating state. This full SWT condition is approximated by the mean-field theory as $B_{cH} \simeq (w-U)/g\mu_B$ for the moderate U/t case and $B_{cH} \simeq \frac{3}{4}J/g\mu_B \simeq \frac{3t^2}{U}/g\mu_B$ for the large U/t case (see method). This explains why the charge gap can be closed when E_z is only a fraction of U for the moderate U/t case. Based on the experimental results shown in Fig. 4a, we can conclude that our system is in the moderate U/t regime when $D \gtrsim 0.15$ V/nm (IMI case) and in the crossover from moderate to large U/t regime when $D \lesssim 0.15$ V/nm (II case). We argue that the observation of the II transition is a direct evidence of this new type of SWT because without SWT the spin-up sub-LHB and spin-down sub-UHB have to overlap with the increase of the magnetic field before the system gets fully polarized, leading to transitions with unavoidable intermediate metallic phase (see Extended Data Fig. 10). The II transition in the crossover regime is consistent with previous studies where the magnetic field can only induce phase transitions with different spin structures in the large U/t regime without closing the charge gap [10–13]. In the whole moderate to large U/t regime, the gap of the insulator at $B > B_{\mathrm{cH}}$ is cooperatively determined by U and E_{Z}, which scales as $U + E_{\mathrm{z}} - w$. This proportional relation is evidenced by our experimental observation as shown in Fig. 3f. These results further highlight correlation effects in such spin-polarized states, which we dub the Mott-Zeeman insulator.

Displacement field and twist angle tuning

Based on the above physical picture, we further show in Fig. 4d the global evolution of the gap versus E_{z} and the layer potential difference ΔV ($\propto D$). Consistent with experimental results, as ΔV increases, the B_{cH} of the IMI/II transitions increase monotonically, resulting from the fact that w also has a linear dependence on ΔV (note $B_{cH} \simeq (w-U)/g\mu_B$ or $B_{cH} \simeq \frac{3t^2}{U}/g\mu_B$ as discussed above). The twist angle also affects w, which decreases quadratically as θ decreases [7]. In Fig. 4e, we plot the calculated B_{cH} as a function of ΔV for different twist angles. Clearly, B_{cH} also decreases with decreasing θ. Overlaying the experimental data (points in Fig. 4e) for multiple devices with θ ranging from 2.4° to 3.2° (see Extended Data Fig. 11 for fan diagrams), we see good agreement between experiment and theory. This trend suggests that for smaller twist angles the IMI/II transitions can be realized at a magnetic field even lower than 5 T.

Conclusion

The transport data on TB-WSe_2 and theoretical calculations presented here provide compelling evidence that the spectral weight transfer is essential for understanding the response of a Mott insulator to magnetic field. As a result of SWT and the reduced U in moiré systems, for the first time we show that the charge degree of freedom can be tuned via magnetic fields in a Mott insulator and subsequently observe Mott insulator to metal to Mott-Zeeman insulator transitions at a Zeeman energy much smaller than U. This unusual magnetic-field-induced evolution is demonstrated to be tunable with both the displacement field and twist angle. As SWT has only been established in the process of doping a Mott insulator before [1, 2, 22, 28, 29], the new type of SWT occurring in the magnetic-field response of a Mott insulator with the charge carrier density fixed at half filling is remarkable. Thus, our findings reveal that the universal characteristics of Mottness are intimately connected to the occupancy properties of Hubbard bands. As doping a Mott insulator can realize high-T_{c} superconductivity [1, 2], our work opens up the possibility to realize exotic correlated superconductivity. In addition, as the ground state of our system could be either ordered or disordered quantum spin phases [30–33], the magnetic-field-induced transitions could provide new avenues to investigate quantum spin liquids.

[1] P. A. Lee, N. Nagaosa, and X.-G. Wen, Rev. Mod. Phys. **78**, 17 (2006).
[2] P. Phillips, Rev. Mod. Phys. **82**, 1719 (2010).
[3] B. Keimer, S. A. Kivelson, M. R. Norman, S. Uchida, and J. Zaanen, Nature **518**, 179 (2015).
[4] Y. Cao, V. Fatemi, A. Demir, S. Fang, S. L. Tomarken, J. Y. Luo, J. D. Sanchez-Yamagishi, K. Watanabe, T. Taniguchi, E. Kaxiras, *et al.*, Nature **556**, 80 (2018).
[5] Y. Cao, D. Rodan-Legrain, O. Rubies-Bigorda, J. M. Park, K. Watanabe, T. Taniguchi, and P. Jarillo-Herrero, Nature **583**, 215 (2020).
[6] X. Liu, Z. Hao, E. Khalaf, J. Y. Lee, Y. Ronen, H. Yoo, D. Haei Najafabadi, K. Watanabe, T. Taniguchi, A. Vishwanath, *et al.*, Nature **583**, 221 (2020).
[7] L. Wang, E.-M. Shih, A. Ghiotto, L. Xian, D. A. Rhodes, C. Tan, M. Claassen, D. M. Kennes, Y. Bai, B. Kim, *et al.*, Nature materials **19**, 861 (2020).

[8] T. Li, S. Jiang, L. Li, Y. Zhang, K. Kang, J. Zhu, K. Watanabe, T. Taniguchi, D. Chowdhury, L. Fu, *et al.*, Nature **597**, 350 (2021).
[9] S. Miao, T. Wang, X. Huang, D. Chen, Z. Lian, C. Wang, M. Blei, T. Taniguchi, K. Watanabe, S. Tongay, *et al.*, Nature communications **12**, 3608 (2021).
[10] J. Zheng, K. Ran, T. Li, J. Wang, P. Wang, B. Liu, Z.-X. Liu, B. Normand, J. Wen, and W. Yu, Phys. Rev. Lett. **119**, 227208 (2017).
[11] Y. Kasahara, T. Ohnishi, Y. Mizukami, O. Tanaka, S. Ma, K. Sugii, N. Kurita, H. Tanaka, J. Nasu, Y. Motome, *et al.*, Nature **559**, 227 (2018).
[12] A. Banerjee, P. Lampen-Kelley, J. Knolle, C. Balz, A. A. Aczel, B. Winn, Y. Liu, D. Pajerowski, J. Yan, C. A. Bridges, *et al.*, npj Quantum Materials **3**, 8 (2018).
[13] Y. Shangguan, S. Bao, Z.-Y. Dong, N. Xi, Y.-P. Gao, Z. Ma, W. Wang, Z. Qi, S. Zhang, Z. Huang, J. Liao, X. Zhao, B. Zhang, S. Cheng, H. Xu, D. Yu, A. Mole, Richard, N. Murai, S. Ohira-Kawamura, L. He, J. Hao, Q.-B. Yan, F. Song, W. Li, S.-L. Yu, J.-X. Li, and J. Wen, Nature Physics (2023), 10.1038/s41567-023-02212-2.
[14] D. M. Kennes, M. Claassen, L. Xian, A. Georges, A. J. Millis, J. Hone, C. R. Dean, N. B. D, A. N. Pasupathy, and A. Rubio, Nature Physics **17**, 155 (2021).
[15] Y. Shimazaki, I. Schwartz, K. Watanabe, T. Taniguchi, M. Kroner, and A. Imamoğlu, Nature **580**, 472 (2020).
[16] T. Li, S. Jiang, B. Shen, Y. Zhang, L. Li, Z. Tao, T. Devakul, K. Watanabe, T. Taniguchi, L. Fu, *et al.*, Nature **600**, 641 (2021).
[17] T. Li, J. Zhu, Y. Tang, K. Watanabe, T. Taniguchi, V. Elser, J. Shan, and K. F. Mak, Nature Nanotechnology **16**, 1068 (2021).
[18] H. C. Movva, B. Fallahazad, K. Kim, S. Larentis, T. Taniguchi, K. Watanabe, S. K. Banerjee, and E. Tutuc, Physical review letters **118**, 247701 (2017).
[19] M. V. Gustafsson, M. Yankowitz, C. Forsythe, D. Rhodes, K. Watanabe, T. Taniguchi, J. Hone, X. Zhu, and C. R. Dean, Nature materials **17**, 411 (2018).
[20] D. Sénéchal, D. Perez, and M. Pioro-Ladrière, Phys. Rev. Lett. **84**, 522 (2000).
[21] S.-L. Yu, X. C. Xie, and J.-X. Li, Phys. Rev. Lett. **107**, 010401 (2011).
[22] W.-H. Leong, S.-L. Yu, T. Xiang, and J.-X. Li, Phys. Rev. B **90**, 245102 (2014).
[23] H. Pan, F. Wu, and S. Das Sarma, Phys. Rev. Res. **2**, 033087 (2020).
[24] J. Zang, J. Wang, J. Cano, and A. J. Millis, Physical Review B **104**, 075150 (2021).
[25] J. Zang, J. Wang, J. Cano, A. Georges, and A. J. Millis, Physical Review X **12**, 021064 (2022).
[26] A. Wietek, J. Wang, J. Zang, J. Cano, A. Georges, and A. Millis, Physical Review Research **4**, 043048 (2022).
[27] L. Klebl, A. Fischer, L. Classen, M. M. Scherer, and D. M. Kennes, Physical Review Research **5**, L012034 (2023).
[28] H. Eskes, M. B. J. Meinders, and G. A. Sawatzky, Phys. Rev. Lett. **67**, 1035 (1991).
[29] C. Ye, P. Cai, R. Yu, X. Zhou, W. Ruan, Q. Liu, C. Jin, and Y. Wang, Nature communications **4**, 1365 (2013).
[30] O. I. Motrunich, Phys. Rev. B **72**, 045105 (2005).
[31] P. Sahebsara and D. Sénéchal, Phys. Rev. Lett. **100**, 136402 (2008).
[32] A. Szasz, J. Motruk, M. P. Zaletel, and J. E. Moore, Phys. Rev. X **10**, 021042 (2020).
[33] D. Kiese, Y. He, C. Hickey, A. Rubio, and D. M. Kennes, APL Materials **10** (2022).

ACKNOWLEDGMENTS

We thank Q. H. Wang, and J. Zang for helpful discussions. L.W. acknowledges the National Key Projects for Research and Development of China (Grant Nos. 2021YFA1400400, 2022YFA1204700), National Natural Science Foundation of China (Grant No. 12074173) and Natural Science Foundation of Jiangsu Province (Grant No. BK20220066). J.-X.L. acknowledges the National Key Projects for Research and Development of China (Grant No. 2021YFA1400400) and the National Natural Science Foundation of China (Grant No. 92165205). D.M.K, A.F. and C.S.W. acknowledge funding by the Deutsche Forschungsgemeinschaft (DFG, German Research Foundation) under RTG 1995, via Germany's Excellence Strategy – Cluster of Excellence Matter and Light for Quantum Computing (ML4Q) EXC 2004/1 – 390534769. A.F, C.S.W., and D.M.K. acknowledge funding by the DFG under RTG 1995, within the Priority Program SPP 2244 "2DMP" — 443273985. L.X. and Q.X. acknowledge the support by the National Key Research and Development Program of China (Grant No. 2022YFA1403501) and the Key-Area Research and Development Program of Guangdong Province of China (Grant No. 2020B0101340001) and the Hefei National Research Center for Physical Sciences at the Microscale (KF2021003) and the Max Planck Partner group programme. The computational resources were provided by the Platform for Data-Driven Computational Materials Discovery of the Songshan Lake Materials Laboratory. K.W. and T.T. acknowledge support from the JSPS KAKENHI (Grant Numbers 21H05233 and 23H02052) and World Premier International Research Center Initiative (WPI), MEXT, Japan. We acknowledge users with Excellence Project of Hefei Science Center CAS, 2021HSC-UE007. We acknowledge support from the Max Planck-New York City Center for Non-Equilibrium Quantum Phenomena. A.R. acknowledges the support by the European Research Council (ERC-2015-AdG-694097), Grupos Consolidados (IT1249-19), SFB925 and by the Deutsche Forschungsgemeinschaft (DFG, German Research Foundation) under Germany's Excellence Strategy - Cluster of Excellence and Advanced Imaging of Matter (AIM) EXC 2056 - 390715994 and RTG 2247. M.C. is supported by a startup grant from the University of Pennsylvania. A.R. is supported by the Flatiron Institute, a division of the Simons Foundation. D.A.R. and Y.H. acknowledge support from the University of Wisconsin-Madison, Office of the Vice Chancellor for Research and Graduate Education with funding

from the Wisconsin Alumni Research Foundation. Simulations were performed with computing resources granted by RWTH Aachen University under project rwth 1258, 1420.

AUTHOR CONTRIBUTIONS

L.N.W. fabricated the samples and performed the transport measurements. L.N.W. and L.W. analyzed the data. D.A.R. and Y.C.H. grew the WSe_2 crystals. K.W. and T.T. grew the hBN crystals. Q.L.X. and L.X. performed the density functional theory calculation. D.M.K., A.F. and C.S.W. performed the mean field theory calculation. Z.-L.G and J.-X.L performed the CPT calculation. J.-X.L., D.M.K and L.D.X. supervised the theoretical aspects of this work. L.N.W., Z.-L.G, J.-X.L, and L.W. wrote the manuscript with input from all the authors.

COMPETING INTEREST DECLARATION

The authors declare no competing interest.

DATA AVAILABILITY

The data that support the findings of this study are available from the corresponding authors upon request.

Supplementary Files

This is a list of supplementary files associated with this preprint. Click to download.

- extendeddata.pdf